NMR structure of the channel-former zervamicin IIB in isotropic solvents

T.A. Balashova[a], Z.O. Shenkarev[a], A.A. Tagaev[a], T.V. Ovchinnikova[a], J. Raap[b], A.S. Arseniev[a,*]

[a] *Shemyakin-Ovchinnikov Institute of Bioorganic Chemistry, Russian Academy of Sciences, ul. Miklukho-Maklaya, 16/10, 117871 Moscow, Russia*
[b] *Leiden Institute of Chemistry, Gorlaeus Laboratories, Leiden University, Einsteinweg 55, P.O. Box 9502, 2300 RA Leiden, The Netherlands*

Received 16 November 1999

Edited by Vladimir Skulachev

Abstract Spatial structure of the membrane channel-forming hexadecapeptide, zervamicin IIB, was studied by NMR spectroscopy in mixed solvents of different polarity ranging from $CDCl_3/CD_3OH$ (9:1, v/v) to CD_3OH/H_2O (1:1, v/v). The results show that in all solvents used the peptide has a very similar structure that is a bent amphiphilic helix with a mean backbone root mean square deviation (rmsd) value of ca. 0.3 Å. Side chains of Trp[1], Ile[2], Gln[3], Ile[5] and Thr[6] are mobile. The results are discussed in relation to the validity of the obtained structure to serve as a building block of zervamicin IIB ion channels.

Key words: Nuclear magnetic resonance; Antibiotic; Zervamicin; Channel-former; Peptaibol

1. Introduction

Zervamicin IIB (Zrv-IIB) belongs to a family of acyclic, α-aminoisobutyric acid containing polypeptides (peptaibols) of fungal origin which form voltage-gated channels in phospholipid bilayer membranes [1]. Zrv-IIB and several other zervamicins were isolated from cultures of *Emericellopsis salmosynnemata* [2]. They are active against Gram-positive bacteria, less active against Gram-negative bacteria and not toxic to eukaryotic cells [2,3]. Zrv-IIB contains 16 amino acid residues, the N-terminus being acetylated (Ac) and the C-terminus is the α-amino alcohol phenylalaninol (Phl): AcTrpIle-GlnIvaIle[5]ThrAibLeuAibHyp[10]GlnAibHypAibProPhl[16] (Aib, α-aminoisobutyric acid; Iva, D-isovaline; Hyp, 4-hydroxyproline; Phl, L-phenylalaninol).

The channel forming properties of Zrv-IIB have been studied [4–6] and a number of models explaining electric properties of the channels were proposed [4–10]. All this models are based on the crystal structures of Leu[1]-Zrv-IIB and an analogue of zervamicin IIA [8–10]. Channels are believed to be formed by bundles of Zrv-IIB helices surrounding a central ion permeable pore. The different conductance levels of Zrv-IIB were ascribed to different numbers of helices per bundle [4,5].

In the present work the spatial structure of Zrv-IIB was studied in organic solvents of different polarity from a very polar (represented by methanol/water (1:1, v/v)) to an essentially non-polar (chloroform/methanol (9:1, v/v)) solvent. Thus the spatial structure was monitored in the different environments ranging from those characteristic of water/phospholipid membrane interface to the hydrocarbon core of the membrane.

2. Materials and methods

2.1. Sample preparation

The *E. salmosynnemata* strain 336 IMI 58330, producing Zrv-IIB was kindly gifted by the Upjohn Co., Kalamazoo, MI, USA. The 96-h seed culture was prepared as in [2] and was grown in a fermentation medium containing 10 g of bacto peptone (Difco), 2.5 g of yeast extract (Difco), 10 g of starch and 8 g of $CaCO_3$ per l (pH 7.2). The culture was shaken at 28°C for 170 h and filtered on a glass filter. The filter cake was triturated with methanol (5 ml/g) and the methanolic extract was dried in vacuo. The solid was dissolved in a minimal volume of methanol and purified by gel filtration chromatography on a Sephadex LH-20 column (2.5×100 cm) using methanol as an eluant (flow rate 0.2 ml/min). The fraction containing a mixture of zervamicins IC, IIA and IIB was further separated by RP-HPLC on a SGX C18 column (8×250 mm, 7 μ) purchased from Separon (Czech Republic). The solutes were eluted by using the ternary mixture methanol/acetonitrile/water (67:14:19, v/v) at a flow rate of 1.6 ml/min. The homogeneous fractions were dried and redissolved in deuterated solvents for nuclear magnetic resonance (NMR) experiments.

2.2. NMR measurements

All NMR experiments were performed on a Varian Unity 600 spectrometer for 10 mM Zrv-IIB in C^2H_3OH, $C^2H_3O^2H$ and binary C^2H_3OH/C^2HCl_3 or C^2H_3OH/H_2O mixtures. 2D double quantum filtered correlated spectroscopy (DQF-COSY) [11], 2D total correlated spectroscopy (TOCSY) [12] with mixing times (τ_m) of 50 and 70 ms and 2D nuclear Overhauser effect-correlated spectroscopy (NOESY) [13] with τ_m's of 200 and 300 ms were recorded in the pure phase-absorption mode by collecting hypercomplex data [14]. The WATERGATE [15] and FLIP-BACK [16] techniques were used for the suppression of strong solvent resonance. A relaxation delay of 3.2 s was used. Chemical shifts were measured relative to the residual C^2H_2H signal of methanol, the chemical shift of the signal being arbitrary chosen as 3.3 ppm relative to tetramethylsilane. Proton spin-spin coupling constants (H-NC^{α}-H and H-$C^{\alpha}C^{\beta}$-H) were measured in 1D spectra with a digital resolution of 0.25 Hz/point. ^{15}N-$C^{\alpha}C^{\beta}$-H Heteronuclear spin-spin coupling constants were measured in the NOESY spectra of 3 mM ^{15}N-labeled Zrv-IIB in C^2H_3OH at 30°C as in [17].

To detect amide protons with slow hydrogen deuterium exchange rates, 1D spectra were recorded starting at 5, 20, 40, 60, 90, 120 and 240 min on a Zrv-IIB solution in $C^2H_3O^2H$, with the apparent pH of 5.8 and at a temperature of 15°C.

*Corresponding author. Fax: (7)-95-3355033.
E-mail: aars@nmr.ru

Abbreviations: NMR, nuclear magnetic resonance; 2D, two-dimensional; NOE, nuclear Overhauser effect; DQF-COSY, 2D double quantum filtered correlated spectroscopy; NOESY, 2D NOE-correlated spectroscopy; rmsd, root mean square deviation; TOCSY, 2D total correlated spectroscopy; Zrv-IIB, zervamicin IIB

PII: S0014-5793(99)01707-X

All NMR spectra were processed and quantified using a macro within the VNMR, Varian software. Complete proton resonance assignment was obtained by a standard procedure [18] using the XEASY program [19]. Cross-peak intensities were measured using an algorithm of a non-linear least squares approximation for lineshapes of cross-peak sections in both directions of the two-dimensional (2D) spectra implemented in the XEASY program.

2.3. Spatial structure calculation

The spatial structure calculation was performed using the DYANA program [20]. Interproton distance constraints were derived from the cross-peak intensities measured in the NOESY spectra with $\tau_m = 200$ ms where spin-diffusion effects might be ignored. 129 Meaningful interproton distance constraints were derived from 355 unambiguously assigned NOESY cross-peak volumes via a '$1/r^6$' calibration. Stereospecific assignments of methylene protons were obtained for residues with the use of the GLOMSA program [21] based on combination of the available spin-spin coupling constants and NOE-derived distance constraints. To eliminate unrealistic conformations and describe the available conformational space to the maximum, we did not constrain those protons or pseudocenters that were affected by the angles for which we could not reject mobility based on spin-spin coupling constants. Pseudoatom constraints were utilized in cases when the stereospecific assignment for prochiral centers was unknown. Twelve torsion angle constraints were derived from spin-spin coupling constants of H-NC$^\alpha$-H (φ angle), H-C$^\alpha$C$^\beta$-H and ^{15}N-C$^\alpha$C$^\beta$-H (χ^1 angle) nuclei, the stereospecific assignments were obtained as described above. The used procedure was essentially as in [22].

After generation of the set of 50 structures confirming the interproton upper distance and torsion angle constraints, 19 additional lower distance constraints (3.0 Å), based on cross-peaks expected (according to the structures obtained) but not present in NOESY spectra, were introduced as described in [23]. Upper (NH...O 2.3 Å, N...O 3.3 Å) and lower (NH...O 1.8 Å, N...O 2.8 Å) distance constraints were introduced for hydrogen bonds detected in more than 30 out of the 50 calculated structures and confirmed by slow hydrogen-deuterium exchange rates of the corresponding amide protons. The next generation of 100 structures was calculated with addition of hydrogen bonds and lower distance constraints and the 20 best of them were selected accounting to the following criteria: (1) each structure differs from all others by root mean square deviation (rmsd) of backbone atom coordinates $\geq$0.05 Å and (2) low final DYANA target function $\leq$0.03 Å^2. Visual analysis of the structures obtained and preparation of the figures were performed using the MOLMOL program [24].

2.4. Energy minimization

In order to prevent bad sterical contacts, the 20 best DYANA structures were subjected to energy minimization using the DISCOVER program [25], the CVFF force field [26], the dielectric constant $\varepsilon = 33$ (close to that of methanol), and the same distance and torsion angle restraints as used on the last stage of DYANA's protocol.

3. Results and discussion

The complete resonance assignment for Zrv-IIB in methanol was obtained using standard procedures on the basis of DQF-COSY, TOCSY and NOESY spectra. A single set of signals in the NMR spectra testifies to the absence of impurities or *cis-trans* X-Pro peptide bond isomers in the sample. The *trans* orientation of the Aib^9-Hyp^{10}, Aib^{12}-Hyp^{13} and Aib^{14}-Pro^{15} peptide bonds was established based on the intensive sequential NOE cross-peaks between C$^\alpha$-CH$_3$ protons of Aib and C$^\delta$H$_2$ protons of the subsequent Pro or Hyp residues.

According to criteria described in [27], pyrrolidine rings of Hyp^{10} and Hyp^{13} residues have a 'Up', while the one of Pro^{15} residue has a 'Twist' conformation.

The Gln^3, Leu^8, Gln^{11} and Phl^{16} residues have one small (3.2–5.0 Hz) and one large (11.4–10.0 Hz) spin-spin coupling constant of H-C$^\alpha$C$^\beta$-H protons, which corresponds to one most populated ($80 \pm 10\%$) χ^1 rotamer ($180 \pm 30°$ or $-60 \pm 30°$). Analysis of ^{15}N-C$^\alpha$C$^\beta$-H spin-spin coupling constants (for each residue one small (0–2 Hz) and one large (3.9–5.9 Hz) $^3J15_{N-C}\alpha_C\beta_{-H}$ value was observed) showed that residues 3, 8, 11 and 16 have the most populated $\chi^1 = -60 \pm 30°$ rotamer.

The averaged (6.2–8.2 Hz) $^3J_{H-C}\alpha_C\beta_{-H}$ values of Trp^1, Ile^2 and Ile^5 correspond to the almost free rotation of the corresponding side chains. The revealed dynamic properties of the Zrv-IIB side chains were taken into account at the spatial structure calculation (see Section 2).

A summary of the NMR data used in the spatial structure calculation is shown in Fig. 1. The structure was calculated on the assumption that a single Zrv-IIB backbone conformation is consistent with all available experimental data. The correctness of this assumption is confirmed by: (1) small constraint violations, (2) small rmsd values (see Table 1) and (3) a scatter plot of φ and ψ torsion angles (Fig. 2) in the obtained set of structures. The results of the spatial structure calculation, by using the program DYANA and the results of energy minimization by application of the program DISCOVER, are collected in Tables 1 and 2, respectively.

The Zrv-IIB spatial structure is shown in Fig. 3. The structure might be characterized as a bent (near by its center, with a bending angle of $\sim$40°) amphiphilic helix. The bent helix is typical for zervamicines [8,9,28] and apparently defined by a high concentration of helix formers (Aib and Iva residues) [29]

Table 1
Structural statistics of the 20 best DYANA structures of Zrv-IIB

Parameter	Quantity	Unit	DYANA
Target function	average ± S.D.	Å^2	0.02 ± 0.005
Number of distance constraints (upper/lower)	NOE		129/19
	H-bond		16/16
Number of torsion angle constraints	angle ϕ		8
	angle χ^1		4
Upper constraint violations	sum ± S.D.	Å	0.25 ± 0.05
	maximum	Å	0.06
Lower constraint violations	sum ± S.D.	Å	0.01 ± 0.005
	maximum	Å	0.01
Van der Waals constraint violations	sum ± S.D.	Å	0.3 ± 0.05
	maximum	Å	0.05
Angle constraint violations	sum ± S.D.	degrees	0.2 ± 0.1
	maximum	degrees	0.1
rmsd of atom coordinates (residues 1–16)	backbone	Å	0.27 ± 0.12
	all heavy atoms	Å	1.48 ± 0.29

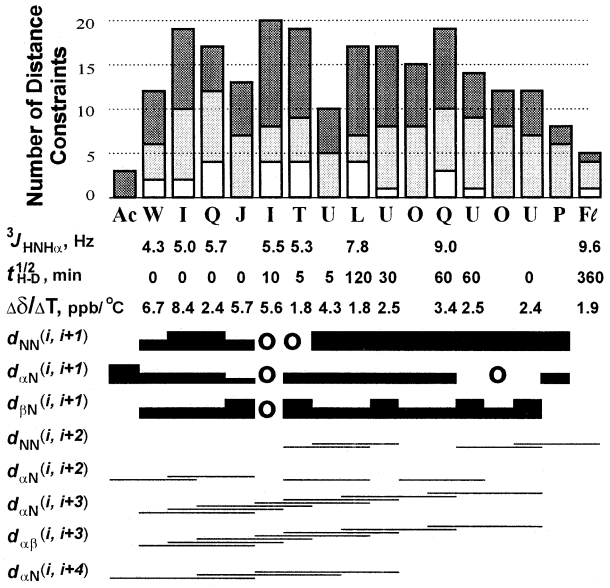

Fig. 1. Overview of NMR data collected for 10 mM Zrv-IIB in methanol at pH 6.2 and 30°C. Amino acid sequence is given in one letter code, where Acetyl, Aib (α-aminoisobutyric acid), Iva (D-isovaline), Hyp (4-hydroxyproline), Phl (α-aminophenilalaninol) are Ac, U, J, O and Fl, respectively and the other residues as usual. The NOE connectivities are denoted as usual: d_{AB} (i,j) is the connectivity between the proton types A and B located in the amino acid residues i and j, respectively. N, α and β denote the amide ($C^{\delta}H_2$ for O^{10}, O^{13} and P^{15} residues), H^{α} (C^{α}-CH_3 for J^4, U^7, U^9, U^{12} and U^{14} residues) and H^{β} protons, respectively. Full-size squares denote a high intensity, half squares a medium and lines a low intensity of corresponding cross-peaks in the NOESY 200-ms spectrum. The circle indicates overlapping cross-peaks. The number of distance constraints used in the structure calculation is shown at the top of the figure. White, light gray and black rectangles correspond to intraresidue, sequential and medium-range ($1 < |i-j| \leq 4$) constraints, respectively. Values of $^3J_{HNC}\alpha_H$ coupling constants, temperature coefficients of chemical shifts of amide proton signals ($\Delta\delta/\Delta T$) and half-exchange times of amide protons with solvent deuterons ($t^{HD}_{1/2}$, zero denotes a half-exchange time less then 5 min) are shown in corresponding lines.

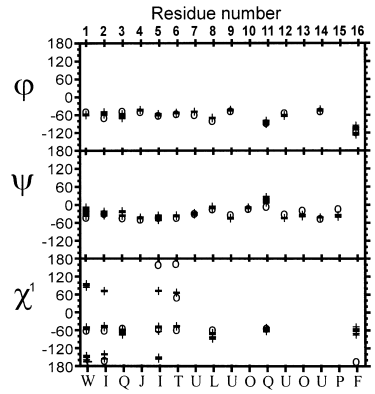

Fig. 2. Scatter plot of the φ, ψ and χ^1 angles for 20 best DYANA structures (after energy minimization) of Zrv-IIB (crosses) and for the crystal form C of Leu[1]-zervamicin X-ray structure (open circles) [9]. Leu[1]-zervamicin differs from Zrv-IIB by replacement of Trp[1] with Leu[1]. The sequence of Zrv-IIB is shown at the bottom.

and proline rich C-termini. Zrv-IIB has polar moieties in the side chains of residues 3 (CO-NH_2 group), 6 (OH), 10 (OH), 11 (CO-NH_2), 13 (OH) and 16 (OH). Additionally, the polar face is enhanced by the exposed carbonyl oxygens in the residues 7 and 10 and amide proton in the residue 14, which do not participate in intramolecular hydrogen bonds. All these polar groups and smaller side chains of the α-aminoisobutyric acids are situated on the convex side of the helix (Fig. 3). The concave surface of the helix is formed by bulky hydrophobic side chains. The only exception of the differentiation is the polar side chain of Gln^{11} which CO-NH_2 group is situated on the otherwise hydrophobic surface of the Zrv-IIB helix. The ends of the helix are also polar due to N-H and CO groups uncompensated by hydrogen bonds.

The N-terminal part of the helix has three i,i+4 type hydrogen bonds (Trp^1 CO...HN Ile^5; Ile^2 CO...HN Thr^6; Gln^3 CO...HN Aib^7) which is characteristic of an α-helix. The C-terminal half of the helix comfortable accommodates two hydroxyprolines (Hyp^{10} and Hyp^{13}) and one proline (Pro^{15}) into a helical β-ribbon stabilized with four hydrogen bonds of the i,i+3 type (Ile^5 CO...HN Leu^8; Thr^6 CO...HN Aib^9; Leu^8 CO...HN Gln^{11}; Aib^9 CO...HN Aib^{12}; approximate 3_{10}-helix with missing hydrogen bonds at Hyp^{10}, Hyp^{13} and Pro^{15}) and one hydrogen bond of i,i+4 type (Aib^{12} CO...HN Phl^{16}). All eight hydrogen bonds found in the Zrv-IIB structure (Fig. 3) are supported by slow deuterium exchange rates and small temperature coefficients of the chemical shifts of the corresponding amide protons. The amide groups of the four N-terminal residues and Aib^{14} do not participate in intramolecular hydrogen bonds being consistent with the fast deuterium exchange rate of the amide groups. The small temperature coefficients of the chemical shifts of Gln^3 and Aib^{14} amide groups remained unexplained.

One of the most interesting questions is related to the orientation and the mobility of the Gln^{11} side chain. In many models of zervamicin channels this side chain either forms intermolecular hydrogen bonds or is involved in ion transport through the pore [8–10]. The absence of NOE's between $C^{\gamma}H_2$ and $CONH_2$ protons of Gln^{11} suggests a fast rotation around C^{β}-C^{γ} and C^{γ}-C^{δ} bonds of the residue.

Detailed knowledge about the Zrv-IIB spatial structure in the membrane bound state(s) is necessary to interpret its mode of action at the molecular level. Clearly the peptides in isotropic solvents are not in a membrane environment. Moreover

Table 2
Statistics of the 20 best DYANA structures before and after DISCOVER energy minimization

Parameter	Unit	Before minimization	After minimization
Total energy	kcal/mol	1127.9 ± 288.8	326.2 ± 6.6
Non-bond repulsion energy	kcal/mol	1671.6 ± 316.3	630.3 ± 9.4
Non-bond dispersion energy (including van der Waals term)	kcal/mol	727.8 ± 26.9	501.7 ± 7.6
Distance+dihedral forcing potential	kcal/mol	34.1 ± 25.6	4.3 ± 0.5
rmsd of backbone atom coordinates (residues 1–16)	Å	0.27 ± 0.12	0.29 ± 0.11
rmsd of all heavy atom coordinates (residues 1–16)	Å	1.48 ± 0.29	1.55 ± 0.30

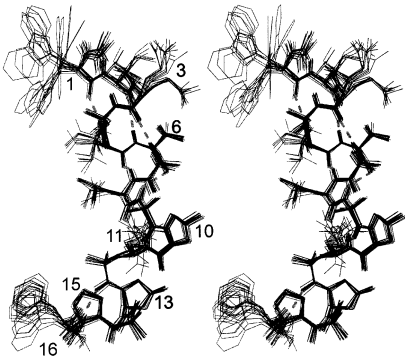

Fig. 3. Stereoview of the 20 best DYANA structures (after energy minimization) of Zrv IIB, superimposed on the backbone atoms of the residues 1–16. Only heavy atoms are shown. Hydrogen bonds are shown in gray dotted lines.

the problem of structure-function relationship for Zrv-IIB became even less tractable taken into account that for the ion channels multilevel conductances has been observed [4,5]. It was suggested that different conductance levels correspond to different numbers of Zrv-IIB monomers forming the channels. In all different channel states the Zrv-IIB monomer is brought into different heterogeneous environments formed from neighboring monomers, lipids, ions and water molecules. The question now arises whether there are significant differences between Zrv-IIB structures of different states? Having this question in mind we investigated the Zrv-IIB spatial structure in mixed solvents of different polarity ranging from methanol/water (1:1, v/v) to methanol/chloroform (1:9, v/v) (further moving out of the specified range of solvent mixtures causes precipitation of the peptide). In the used solvent systems the chemical shifts of aliphatic and aromatic protons as well as the spin-spin coupling constants of the H-NC$^{\alpha}$-H and H-C$^{\alpha}$C$^{\beta}$-H protons of Zrv-IIB were essentially conserved. In case of the backbone amide protons significant upfield shifts were observed only for the solvent exposed amide groups of Trp^{1}, Ile^{2} (ca. 0.7–0.5 ppm) and to a lesser degree those of Gln^{3}, Iva^{4} and Aib^{14} (0.2–0.1 ppm) when the solvent was changed from pure methanol to methanol/chloroform (1:9, v/v). All other backbone amide protons display only small ($\pm$0.05 ppm) changes of the chemical shifts in the used mixed solvents. A detailed comparison of the 200 ms NOESY spectra of Zrv-IIB in methanol/water (1:1, v/v), pure methanol and methanol/chloroform (1:9, v/v) did not reveal changes in the patterns of the NOE cross peaks. All these data establish that the Zrv-IIB structure shown in Fig. 3 is valid to the defined accuracy (see Tables 1 and 2) for a wide variety of solvent systems. It is interesting to note that even crystallization (i.e. close packing of monomers) leads to only small changes of the backbone angles of Zrv-IIB (Fig. 2).

In conclusion, the identity of Zrv-IIB spatial structure in solvents of different polarity and its close similarity to the structure of Leu^{1}-Zrv-IIB in crystal provide strong evidence that it might serve as a building block for molecular modelling of Zrv-IIB ion channels which in turn might be related to their functional (electrical) properties. Overall, the identity of Zrv-IIB structure in the different media mimicking a water/bilayer interfacial region (water/methanol mixtures) and a hydrocarbon core of the membrane (chloroform/methanol mixtures) strongly supports a model in which a voltage dependent step of channel formation does not effect spatial structure of Zrv-IIB (see Fig. 3) but includes reorientation of Zrv-IIB helices from the surface to the transmembrane location. After that the transmembrane oriented Zrv-IIB helices associate into bundles which might be accompanied by some ordering of the otherwise mobile side chains.

Acknowledgements: This work was (financially) supported in part by the Netherlands Organization for Scientific Research (NWO) Project 047.006.009 and by the Ministry of Science and Technology of Russian Federation. We are grateful to Dr. D.A. Skladnev and E.V. Rogozhkina (State Scientific Center of Russian Federation 'GNIIGENETIKA') who prepared the uniformly ^{15}N-labeled Zrv-IIB.

References

[1] Sansom, M.S.P. (1991) Prog. Biophys. Mol. Biol. 55, 139–235.
[2] Argoudelis, A.D., Dietz, A. and Johnson, L.E. (1974) J. Antibiot. 27, 321–328.
[3] Argoudelis, A.D. and Johnson, L.E. (1975) United States Patent 3907990.
[4] Agarwalla, S., Mellor, I.R., Sansom, M.S.P., Karle, I.L., Flippen-Anderson, J.L., Uma, K., Krishna, K., Sukumar, M. and Balaram, P. (1992) Biochem. Biophys. Res. Commun. 186, 8–15.
[5] Balaram, P., Krishna, K., Sukumar, M., Mellor, I.R. and Sansom, M.S.P. (1992) Eur. Biophys. J. 21, 117–128.
[6] Kropacheva, T.N. and Raap, J. (1999) FEBS lett., accepted for publication.
[7] Sansom, M.S.P., Balaram, P. and Karle, I.L. (1993) Eur. Biophys. J. 21, 369–383.
[8] Karle, I.L., Flippen-Anderson, J.L., Agarwalla, S. and Balaram, P. (1991) Proc. Natl. Acad. Sci. USA 88, 5307–5311.
[9] Karle, I.L., Flippen-Anderson, J.L., Agarwalla, S. and Balaram, P. (1994) Biopolymers 34, 721–735.
[10] Karle, I.L. (1996) Biopolymers 40, 157–180.
[11] Rance, M., Sorensen, O.W., Bodenhausen, G., Wagner, C., Ernst, R.R. and Wuthrich, K. (1983) Biochem. Biophys. Res. Commun. 117, 479–485.
[12] Bax, A. and Davis, D.G. (1985) J. Magn. Reson. 65, 355–366.
[13] Jeener, J., Meir, G.N., Bachman, P. and Ernst, R.R. (1979) J. Chem. Phys. 71, 4546–4553.
[14] States, D.J., Habercorn, R.A. and Ruben, D.J. (1982) 48, 286–292.
[15] Piotto, M., Sauder, V. and Sklenar, V. (1992) J. Biomol. NMR 2, 661–665.
[16] Lippens, J., Dhalluin, C. and Wieruszeski, J.-M. (1995) J. Biomol. NMR 5, 327–331.
[17] Montelione, G.T., Winkler, M.E., Rauenbuehler, P. and Wagner, G. (1989) J. Magn. Reson. 82, 198–204.
[18] Wuthrich, K. (1986) NMR of Proteins and Nucleic Acids, John Wiley and Sons, New York.
[19] Bartels, C., Xia, T.-H., Billeter, M., Guntert, P. and Wuthrich, K. (1995) J. Biomol. NMR 6, 1–10.
[20] Guntert, P., Mumenthaler, C. and Wuthrich, K. (1997) J. Mol. Biol. 273, 283–298.
[21] Guntert, P., Braun, W. and Wuthrich, K. (1991) J. Mol. Biol. 217, 517–530.
[22] Dementieva, D.V., Bocharov, E.V. and Arseniev, A.S. (1999) Eur. J. Biochem. 263, 152–162.
[23] Jaravine, V.A., Nolde, D.E., Reibarkh, M.J., Korolkova, Yu.V., Kozlov, S.A., Pluzhnikov, K.A., Grishin, E.V. and Arseniev, A.S. (1997) Biochemistry 36, 1223–1232.
[24] Koradi, R., Billeter, M. and Wuthrich, K. (1996) J. Mol. Graph. 14, 51–55.
[25] Insight II User Guide, version 2.1.0. San Diego: Biosym Technologies, 1992.
[26] Dauber-Osguthorpe, P., Roberts, V.A., Osguthorpe, D.J., Wolff, J., Genest, M. and Hagler, A.T. (1988) Proteins Struct. Funct. Genet. 4, 31–47.
[27] Cai, M., Huang, Y., Liu, J. and Krishnamoorthi, R. (1995) J. Biomol. NMR 6, 123–128.
[28] Karle, I.L., Flippen-Anderson, J.L., Sukumar, M. and Balaram, P. (1987) Proc. Natl. Acad. Sci. USA 84, 5087–5091.
[29] Karle, I.L. and Balaram, P. (1990) Biochemistry 29, 6747–6756.